First-principles study of Ce^{3+}-doped lanthanum silicate nitride phosphors: Neutral excitation, Stokes shift, and luminescent center identification

Yongchao Jia,[1,*] Anna Miglio,[1] Samuel Poncé,[1] Xavier Gonze,[1] and Masayoshi Mikami[2]

[1]*European Theoretical Spectroscopy Facility, Institute of Condensed Matter and Nanosciences, Université catholique de Louvain, Chemin des étoiles 8, bte L07.03.01, B-1348 Louvain-la-Neuve, Belgium*

[2]*MCHC R&D Synergy Center, Inc., 1000, Kamoshida-cho Aoba-ku, Yokohama, 227-8502, Japan*

(Received 20 November 2015; published 6 April 2016)

We study from first principles two lanthanum silicate nitride compounds, $LaSi_3N_5$ and $La_3Si_6N_{11}$, pristine as well as doped with Ce^{3+} ion, in view of explaining their different emission color, and characterizing the luminescent center. The electronic structures of the two undoped hosts are similar, and do not give a hint to quantitatively describe such difference. The $4f \rightarrow 5d$ neutral excitation of the Ce^{3+} ions is simulated through a constrained density functional theory method coupled with a ΔSCF analysis of total energies, yielding absorption energies. Afterwards, atomic positions in the excited state are relaxed, yielding the emission energies and Stokes shifts. Based on these results, the luminescent centers in $LaSi_3N_5$:Ce and $La_3Si_6N_{11}$:Ce are identified. The agreement with the experimental data for the computed quantities is quite reasonable and explains the different color of the emitted light. Also, the Stokes shifts are obtained within 20% difference relative to experimental data.

DOI: 10.1103/PhysRevB.93.155111

I. INTRODUCTION

Phosphors are essential components of white light-emitting-diodes (LEDs). In particular, phosphors activated by the Ce^{3+} ion, presenting a $4f \rightarrow 5d$ spin-allowed transition, have attracted much attention from academia and industry. A large effort has been devoted to the development of novel Ce^{3+} doped systems in the last decades [1–6]. However, most of these have been found thanks to a semiempirical method [7–9] that can only provide trends and qualitative predictions. Especially, the prediction on emission property and Stokes shift is limited since the structure geometry of excited state is difficult to measure experimentally. A typical example beyond the expectation of the semiempirical method is the emission color of Ce^{3+} ion in two closely related lanthanum silicon nitrides (LSN), $LaSi_3N_5$ and $La_3Si_6N_{11}$. In particular, the latter is a blue-convertible yellow phosphor, with a great potential to replace commercial YAG:Ce, while the former gives a blue emission under the UV excitation.

The crystal structure of $LaSi_3N_5$ was studied by Inoue in 1980 [10]. Its structure is built up of SiN_4 tetrahedra, which are linked by shared corners. In this compound, there is only one nonequivalent La^{3+} crystallographic site. The crystal structure of $Ln_3Si_6N_{11}$ (Ln: lanthanide element) was reported by Woike and Jeitschko in 1995 [11], and that of $La_3Si_6N_{11}$ has recently determined by Yamane's group [12]. Similar to the structural character of $LaSi_3N_5$, the crystal structure of $La_3Si_6N_{11}$ also consists of corner-sharing SiN_4 tetrahedra. $La_3Si_6N_{11}$ crystallizes in a tetrahedral structure with the space group of $P4bm$. In this compound, there are two nonequivalent La^{3+} crystallographic sites. Both sites are coordinated with eight nitrogen atoms, and we call them La_{2a} and La_{4c} according to their Wyckoff positions. The La_{2a} site has a fourfold local symmetry, while the symmetry at the La_{4c} site is lower (as seen in Fig. 1).

In recent years, Ce^{3+} doped LSN samples have been synthesized to examine their potential in solid state lighting applications. The optical performance of $LaSi_3N_5$:Ce was experimentally studied in detail [13,14]. These results show that the Ce^{3+} ion occupies the La^{3+} crystallographic site, and gives the above-mentioned blue emission under UV excitation. On the other hand, the properties of $La_3Si_6N_{11}$:Ce were investigated by Seto *et al.* [15], who found the yellow emission of $La_3Si_6N_{11}$:Ce. This experimental observation has been recently confirmed by Seshadri's group [16]. According to these facts, some preliminary discussions based on crystal structure and dielectric properties have been given to understand the difference between $LaSi_3N_5$:Ce and $La_3Si_6N_{11}$:Ce [16–18]. However, there are still two main questions existing now, which the semiempirical method cannot answer: (1) why do Ce^{3+} ions emit different colors in the two LSN phosphors and (2) which site is the luminescent center in the $La_3Si_6N_{11}$:Ce phosphor?

At present, first-principles calculations have been widely used in material science, as they provide an useful insight in the chemical and electronic properties of materials and hence can aid in the search for better materials or guide modification of existing ones [19–24]. Compared to the semiempirical model, they might also have advantages in the design of phosphors: first, such theoretical simulations can provide a detailed understanding of interactions and effects involved in the optical processes; second, without relying on empirical information they have the potential to precisely simulate $4f \rightarrow 5d$ neutral transition in new potential materials, not only for the absorption process but also for the emission process. Still, a routine use of first-principles methods might not yield the sought understanding. As an example, a recent first-principles study of $LaSi_3N_5$, doped with Ce as well as some other dopant ions, has been published [25]. The hybrid functional HSE06 has been used. They point out that, in their scheme, simply based on the Kohn-Sham band structure, the Ce_{5d} states are in the conduction band, at variance with experimental data.

*yongchao.jia@uclouvain.be

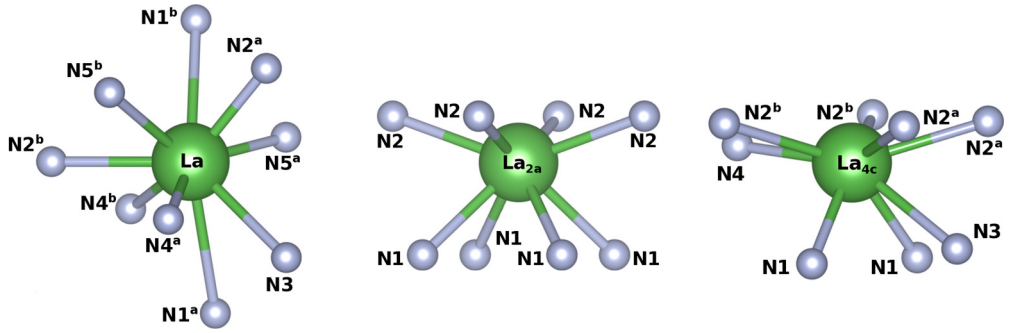

FIG. 1. Coordination environment of (a) the La^{3+} crystallographic site in $LaSi_3N_5$; (b) the La_{2a} site in $La_3Si_6N_{11}$; and (c) the La_{4c} site in $La_3Si_6N_{11}$. Green and gray spheres stand for La and N atoms, respectively.

With this background, in the present study, we have performed an *ab initio* study of these two LSN phosphors, aiming at answering the above-mentioned questions. Our methodological approach differs from the previous *ab initio* study [25], at three levels: (1) constrained DFT allows us to obtain the Ce_{5d} state below the conduction band, in agreement with experimental data; (2) ΔSCF method is used to get the $4f \rightarrow 5d$ transition energy of the Ce^{3+} ion; and (3) the lattice relaxation in the excited state is considered, yielding the Stokes shift and characterization of the Ce^{3+} luminescence. Our paper is structured as follows. In Sec. II, we summarize the calculation method. The study of the undoped LSN bulk materials is presented in Sec. III. The Ce^{3+} doped calculations are shown in Sec. IV, and we give the conclusion in Sec. V.

II. NUMERICAL APPROACH

A. Computational details

In this work, the calculations were performed within density functional theory (DFT) using the projector augmented wave (PAW) method as implemented in the ABINIT package [26–29]. Exchange-correlation (XC) effects were treated within the generalized gradient approximation (GGA) [30]. For the Ce^{3+} doped calculation, DFT+U was used, allowing the Ce_{4f} states to be located inside the band gap [31]. The U value has been optimized to 4.6 eV ($J = 0.5$ eV), in order to reproduce the location of the $4f$ inside the gap, following the hybrid functional study of $LaSi_3N_5$:Ce^{3+} [25]. Because of the similar composition of the two nitrides, the same $U(J)$ value was also used in the study of $La_3Si_6N_{11}$:Ce^{3+}.

Most of the PAW atomic data sets were directly taken from the ABINIT website [32]. The nitrogen data set, with $2s^22p^3$ valence electrons, has a 1.3 Bohr radius and two projectors per angular momentum channel. The silicon PAW data set, with $3s^23p^2$ valence electrons, has a 1.71 Bohr sphere radius and two projectors per angular momentum channel. The cerium data set, with $5s^25p^66s^25d^14f^1$ valence electrons, has a 2.5 Bohr radius and two projectors per angular momentum channel.

For La, we tested two different PAW atomic data sets. The normal ABINIT La PAW dataset, with $5s^25p^66s^25d^14f^0$ as valence electrons, has a 2.5 Bohr sphere radius and two projectors per angular channel. Here, we call this La PAW atomic data set "La_{4f} semicore." In order to test the effect of La_{4f} orbitals, we have generated a PAW atomic data set with the valence configuration $5s^25p^66s^25d^1$ (freezing the unoccupied $4f$ orbital in the core). Here we denote this PAW atomic dataset as "La_{4f} core." The PAW atomic data set was generated using the ATOMPAW software with the same input parameter as the other La PAW GGA-PBE atomic data set, but with frozen $4f$ states.

With these PAW atomic data sets, we performed the structural relaxation and band structure calculations. The convergence criteria have been set to 10^{-5} Ha/Bohr (for residual forces) and 0.5 mHa/atom (for the tolerance on the total energy). In these calculations, cutoff kinetic energies of 30 and 25 Ha for the plane-wave basis set were used for the $LaSi_3N_5$(:Ce) and $La_3Si_6N_{11}$(:Ce) compounds, respectively. The Monkhorst-Pack sampling of the primitive cells (36 atoms for $LaSi_3N_5$ and 40 atoms for $La_3Si_6N_{11}$) for the same tolerance criteria were determined to be $3 \times 3 \times 2$ and $3 \times 3 \times 3$ for the two nitrides, respectively.

B. Supercell calculations

The Ce^{3+} doped LSN calculations have been conducted using the supercell method. The cluster approach based on Hartree-Fock theory was not considered since previous studies have shown this method may lead to the deficiencies of the local geometry around the rare-earth site [33,34]. Moreover, the obvious demerit of the cluster method is the lack of the electronic information about the host lattice. We will see that the position of the conduction band minimum (CBM) of the host is important in the luminescent center identification. Therefore a 72-atom $2 \times 1 \times 1$ supercell for $LaSi_3N_5$ and a 80-atom $1 \times 1 \times 2$ supercell for $La_3Si_6N_{11}$ have been used for the study of Ce^{3+}-doped phosphor. In the calculations, one cerium atom substitutes one lanthanum atom, which leads to $La_7CeSi_{24}N_{40}$ for $LaSi_3N_5$:Ce, and two different cases, $La_{11}Ce_{2a}Si_{24}N_{44}$ and $La_{11}Ce_{4c}Si_{24}N_{44}$, for $La_3Si_6N_{11}$:Ce. Such supercells have a Ce^{3+} doping concentration of 12.5% and 8.3% for the two LSN phosphors, respectively, which is reasonable compared to the experimental data [13,15].

C. Neutral excitations

At present, the Bethe-Salpeter equation (BSE) [35] is the best approach to study the optical properties of solids. It describes neutral excitations as coherent superpositions

of electron-hole pairs. However, the computational burden of such an approach is quite heavy, and not feasible with supercells of nearly one hundred atoms. Instead of BSE, we simulated the $4f \rightarrow 5d$ neutral excitation of Ce^{3+} ion on the basis of the constrained DFT method (CDFT). The electron-hole interaction, an essential contribution in the BSE, is mimicked by promoting the Ce_{4f} electron to the Ce_{5d} state, by constraining the seven $4f$ bands to be unoccupied, while occupying the lowest $5d$ state lying higher in energy. The CDFT method has been used for the search of novel scintillators, proposed by Canning, Chaudhry, and coworkers [36–38]. However, the previous works aimed at the qualitative description of the RE_{5d} state. Compared to these results, we observe the CDFT ability to yield quantitative predictions following the ΔSCF method [39–41], that is, relying on total energy differences of the different constrained configurations. Through the combination of CDFT and ΔSCF, the $4f \rightarrow 5d$ neutral excitation of Ce^{3+} ion is correctly described within the DFT framework, which has a much lower computational cost than the BSE method. In practice, the calculations are performed by setting manually the energy-ordered occupation numbers (optional independent input variables in ABINIT) to one or zero. For both the ground and the excited states, all valence levels, spin up as well as spin down, are occupied. For the ground state, additionally, the lowest spin-up level found in the band gap (clearly identified as a predominantly Ce-$4f$ level) is occupied, while for the excited neutral state, the seven spin-up predominantly Ce-$4f$ levels that are found in the band gap are unoccupied, and the next spin-up level is occupied. In most cases, the latter level is detached from the conduction band, and exhibits Ce-$5d$ character, as will be seen later.

D. Configurational coordinate diagram

Following the proposed method to describe the neutral excitation of Ce^{3+} ion, we will use the configuration coordinate diagram [42] to analyze the absorption/emission process and Stokes shift of the two Ce^{3+}-doped lanthanum silicate nitride phosphors, as shown in Fig. 2.

Here, we briefly explain its physical meaning. This configurational coordinate diagram depicts the total energy of a system containing Ce^{3+} ion in its ground state and of a system containing Ce^{3+} ion in its excited state, curve $4f$ and $5d$, respectively, as a function of the generalized configuration coordinate Q, which can be made up of any relevant combination of ionic degrees of freedom in the system. Q_0 and Q represent the equilibrium configuration coordinates, for the system with Ce^{3+} in its ground and in its excited states, respectively. The horizontal lines inside the curves $4f$ and $5d$ denote the energy levels of the system in which the quantization of vibrational motion is taken into account. When a photon is absorbed by the Ce_{4f} electron, the Ce^{3+} ion will be excited from the ground state to the excited state, corresponding to $A_0 \rightarrow A_0^*$. After the absorption, the system will be out of equilibrium due to the change of electronic configuration of the Ce^{3+} ion. The atomic positions are then relaxed following the forces, which is represented by the process $A_0^* \rightarrow A^*$ in Fig. 2. After this lattice relaxation, the system reaches the new equilibrium state, at which the emission process $A^* \rightarrow A$ occurs. The cycle is finished by the lattice relaxation $A \rightarrow A_0$ process in the ground state. Based on this idea, the absorption/emission energy and the Stokes shift of Ce^{3+}-doped phosphors can be determined as below:

$$E_{\text{abs}} = E_0^* - E_0, \tag{1}$$

$$E_{\text{em}} = E^* - E, \tag{2}$$

$$\Delta S = E_{\text{abs}} - E_{\text{em}}. \tag{3}$$

These values can be directly compared with experimental data, which can validate the proposed method and yield the identification of the luminescence site.

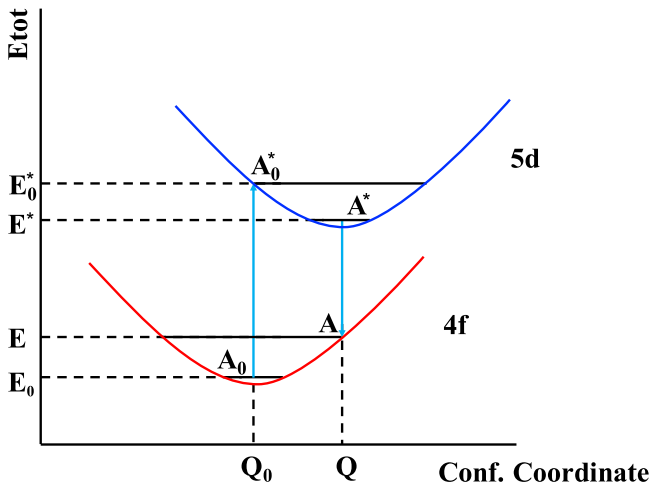

FIG. 2. Configurational coordinate diagram.

III. THE PRISTINE HOSTS

In this section, we focus on the results for bulk $LaSi_3N_5$ and $La_3Si_6N_{11}$: relaxed crystal structure, electronic band structure, and the role of the La_{4f} state in the calculation.

A. Crystal structure

In Sec. I, we have briefly mentioned that $LaSi_3N_5$ is built of SiN_4 tetrahedra, which are linked by shared corners. The La atom is centrally located between the pentagonal holes along the c axis, and is coordinated with nine nitrogen atoms at a distance between 2.6–3.2 Å. $LaSi_3N_5$ crystallizes in the orthorhombic crystal system with space group $P2_12_12_1$.

The space group of $La_3Si_6N_{11}$ is more symmetric, $P4bm$. $La_3Si_6N_{11}$ is isostructural with $Ce_3Si_6N_{11}$. Similar to the structural character of $LaSi_3N_5$, the crystal structure of $La_3Si_6N_{11}$ also consists of corner-sharing SiN_4 tetrahedra. The experimental data [10,12] have been used to start the initial optimization of the crystal structure (with the La_{4f}-semicore PAW atomic data set). Table I lists the relaxed lattice parameters for the two nitride compounds. The theoretical results for LSN bulk are consistent with the experimental value, within 2% relative difference. This small difference might be attributed to the GGA exchange and correlation functional. Figure 3 shows the optimized crystal structure of the two nitrides. One can see that both compounds are composed of corner-sharing SiN_4 tetrahedra, that form a dense network with

TABLE I. Lattice parameters of LSN bulk.

LSN	a (Å)	b (Å)	c (Å)
$LaSi_3N_5$, calc.	4.834	7.891	11.387
$LaSi_3N_5$, exp. [10]	4.807	7.838	11.236
$La_3Si_6N_{11}$, calc.	10.246	10.246	4.887
$La_3Si_6N_{11}$, exp. [12]	10.199	10.199	4.841

large voids accommodating the La^{3+} ions. Figure 1 depicts the relaxed coordinate environments of La^{3+} ion in the two nitrides: one La^{3+} site in $LaSi_3N_5$, and two nonequivalent La^{3+} sites, La_{2a} and La_{4c} sites in $La_3Si_6N_{11}$. When doped, the Ce^{3+} ion is expected to substitute these crystallographic sites, which results in one case of Ce_{La} for $LaSi_3N_5$, and two cases (Ce_{2a} and Ce_{4c}) for $La_3Si_6N_{11}$ with the Ce ion occupying the La_{2a} and La_{4c} sites, respectively. Table II lists the relaxed La-N bond lengths for the three La^{3+} crystallographic sites. Through these results, the average distance of La-N has been determined to be 2.819 Å for the La site in the $LaSi_3N_5$, and 2.711/2.655 Å for the La_{2a}/La_{4c} site in the $La_3Si_6N_{11}$ compound.

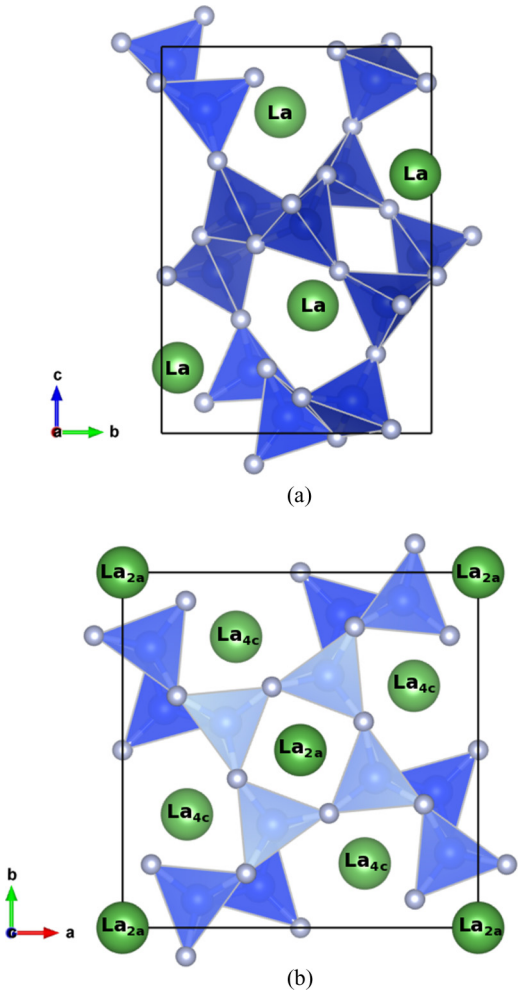

FIG. 3. Crystal structure of (a) $LaSi_3N_5$, view from a direction and (b) $La_3Si_6N_{11}$, view from c direction. Green, blue, and gray spheres stand for La, Si, and N atoms, respectively.

TABLE II. Relaxed La-N bond lengths (Å) of the La crystallographic site in $LaSi_3N_5$ and $La_3Si_6N_{11}$.

Bond	GGA-PAW	Exp. [10,12]
	$LaSi_3N_5$	
La-N1^a	3.151	3.134
La-N1^b	3.140	3.067
La-N2^a	2.443	2.421
La-N2^b	2.724	2.697
La-N3	2.884	2.832
La-N4^a	2.577	2.553
La-N4^b	2.898	2.884
La-N5^a	2.693	2.645
La-N5^b	2.860	2.830
	$La_3Si_6N_{11}$	
La_{2a}-N1(x4)	2.652	2.650
La_{2a}-N2(x4)	2.659	2.644
La_{4c}-N1(x2)	2.528	2.551
La_{4c}-N2^a(x2)	2.674	2.674
La_{4c}-N2^b(x2)	2.893	2.853
La_{4c}-N3	2.823	2.863
La_{4c}-N4	2.640	2.623

The nomenclature for the neighboring nitrogen atoms is presented in Fig. 1. This will help understand the different types of bonds presented in Table II. In $LaSi_3N_5$, there are five types of nitrogen atoms, while the lanthanum atom has nine neighbors. Some symmetry operations do not leave the lanthanum site unchanged. So, among the nine nearest-neighbor atoms of lanthanum, there are four pairs of equivalent nitrogen atoms (by symmetry), whose distance to the specific nitrogen atom differs. The local geometry of La^{3+} site can be represented as a tricapped trigonal prism. In the more symmetric $La_3Si_6N_{11}$, there are four types of nitrogen atoms. The tetragonal symmetry leaves the La_{2a} site unchanged, and the eight nearest-neighbor nitrogen atoms of this site are split in two groups of four, where the La-N distances in each are equal. The La_{4c} site is left unchanged by a mirror plane, so that five distances characterize the locations of the eight nearest-neighbour atoms. The local geometry of La_{2a} and La_{4c} sites can be seen as a square antiprism and a bicapped trigonal prism, respectively.

B. Electronic band structure

With the relaxed crystal structure of the two nitrides, we have calculated the corresponding electronic band structure within the DFT framework, as it might have a bearing on the different luminescent behaviors. Figure 4 shows the calculated results for the La_{4f}-semicore PAW atomic dataset. $LaSi_3N_5$ has a 3.21-eV Γ-X indirect band gap, and $La_3Si_6N_{11}$ belongs to the direct-transition class of compounds with a 2.99-eV band gap at the Z point. At present, there is no experimental data for the band gap of the two compounds. However, we can expect that our calculation suffers from the well-known "band-gap problem" of DFT, with sizable underestimation compared to experimental results. Recently, Ibrahim *et al.* have investigated the electronic structure of $LaSi_3N_5$ using the HSE06 functional, for which the band gap problem is much

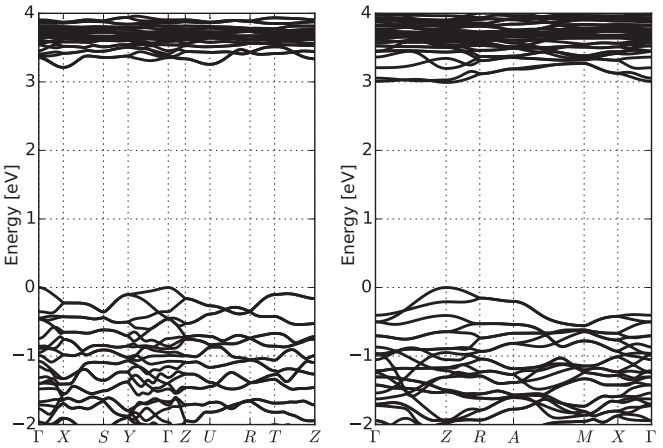

FIG. 4. Kohn-Sham DFT electronic band structure of LSN bulk with converged lattice parameters. $LaSi_3N_5$ (left) and $La_3Si_6N_{11}$ (right).

reduced compared to our GGA approach, giving a band gap of 4.8 eV [25]. In Ref. [16], a similar work for $La_3Si_6N_{11}$ was conducted by Seshadri's group. A band gap of about 4 eV was obtained for this compound. Thus the band gap seems consistently smaller in $La_3Si_6N_{11}$ than in $LaSi_3N_5$. A previous work of one of us was devoted to understand the origin of the change of band gaps, and tried to link it with the optical performance of Ce^{3+} ion in the two compounds [18]. Here, we continue the study, aiming at providing a quantitative description about the performance of the two phosphors.

The composition of the valence-band maximum (VBM) and conduction-band minimum (CBM) might also be important to understand the luminescence. We have examined the partial density of states, as shown in Fig. 5. The results show that for both compounds, the CBM consists of a mixture of La_{4f} and La_{5d} states, while the VBM mainly comes from N_{2p} states. Such similarity again does not help to quantitatively explain the observed different optical properties of LSN phosphors.

To confirm the CBM composition of LSN bulk, the pseudopotential La_{4f} core has been used in band structure calculations. Figure 6 depicts the obtained band structure with the La_{4f}-core PAW atomic data set (still with the relaxed geometry from the lattice relaxation based on La_{4f}-semicore PAW data set). Through comparison of the Figs. 4 and 6, it can be seen that the $4f$ freezing does not modify the valence band, but clearly impacts the conduction band because of the missing $4f$ state in the La_{4f}-core case. The modification of the conduction band leads to small changes of band gap, the one of $LaSi_3N_5$ becomes 3.34 eV and the one of $La_3Si_6N_{11}$ becomes 2.91 eV. From these results, it can be deduced that the La_{4f} state should be considered into our *ab initio* calculation, in order to provide accurate results for the CBM and CBM-related states.

IV. CERIUM-DOPED MATERIALS

The above bulk study has provided the basic information for the two LSN compounds. In this section, the results of Ce^{3+} doped calculations will be presented, including the ground state of the supercell, the excited state description, the effect

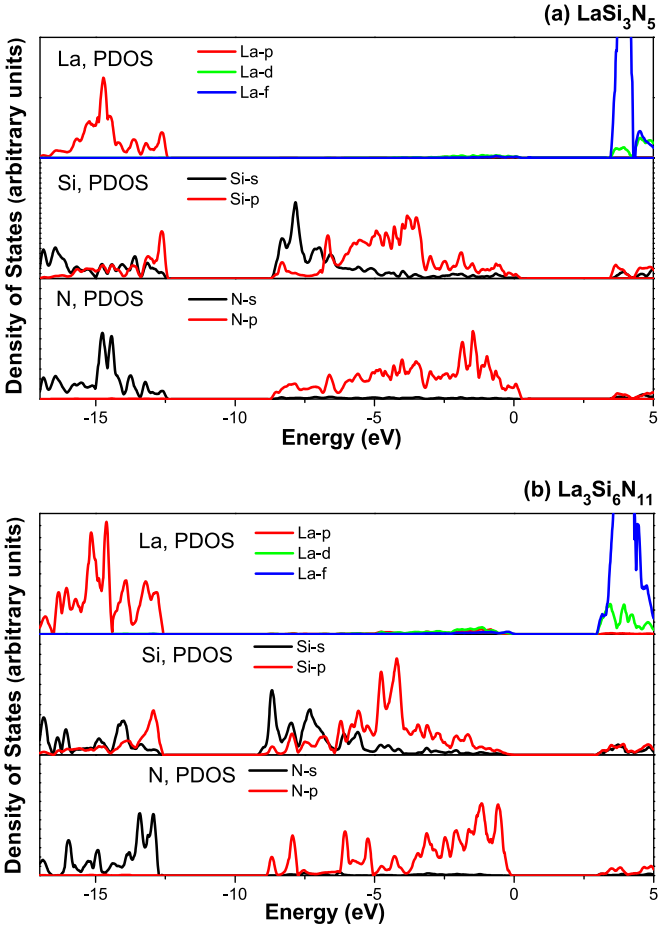

FIG. 5. Partial density of states of (a) $LaSi_3N_5$ and (b) $La_3Si_6N_{11}$

of lattice relaxation in the excited state and the luminescent center identification. The supercells used in this part, namely $La_7CeSi_{24}N_{40}$, $La_{11}Ce_{2a}Si_{24}N_{44}$, and $La_{11}Ce_{4c}Si_{24}N_{44}$, will be simply denoted as $LaSi_3N_5$:Ce, $La_3Si_6N_{11}$:Ce_{2a}, and $La_3Si_6N_{11}$:Ce_{4c}.

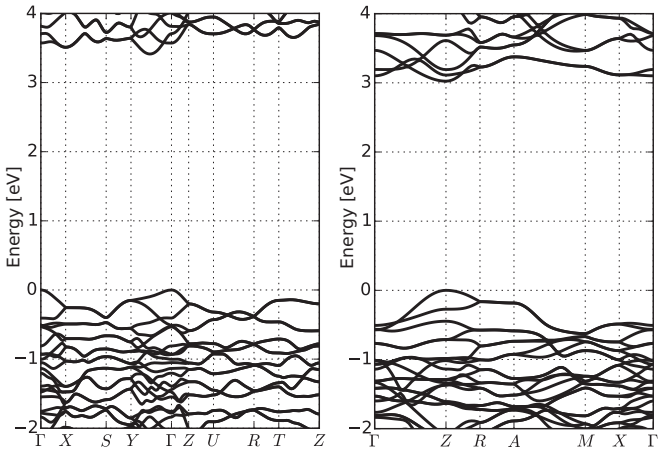

FIG. 6. Kohn-Sham DFT electronic band structure of LSN bulk, in which the $4f$ orbital contributions have been removed, thanks to the use of a PAW atomic dataset in which they are present in the core (La_{4f} core). The structural properties are the same as in Fig. 4 for $LaSi_3N_5$ (left) and $La_3Si_6N_{11}$ (right).

TABLE III. Relaxed lattice parameters (Å) and volume (Å^3) of LSN:Ce supercell.

LSN	Volume (Å^3)	a (Å)	b (Å)	c (Å)
$LaSi_3N_5$	868.77	9.668	7.891	11.387
$LaSi_3N_5$:Ce	867.32	9.662	7.890	11.376
$La_3Si_6N_{11}$	1026.16	10.246	10.246	9.774
$La_3Si_6N_{11}$:Ce_{2a}	1025.78	10.244	10.244	9.774
$La_3Si_6N_{11}$:Ce_{4c}	1025.37	10.243	10.243	9.772

A. Ground state

As mentioned in Sec. II, the analysis of the Ce^{3+} luminescence will be based on the configurational coordinate diagram. Therefore we first focus our attention on the ground state properties. Table III lists the relaxed lattice parameters of the supercells. The data for the corresponding LSN bulk supercells are also shown for comparison, which is obtained from the calculation results for the LSN primitive cell but doubled in the a direction for $LaSi_3N_5$, and in the c direction for $La_3Si_6N_{11}$. From these results, we see that the Ce^{3+} doping leads to a slight shrinkage of the crystal cell. The reason for the contraction can be ascribed to the relatively smaller ionic radius of Ce^{3+} ion than the one of La^{3+} ion . The ionic radius of Ce^{3+} is determined to 1.143 and 1.196 Å for the coordination number of 8 and 9, respectively, while the corresponding values for the La^{3+} ion are 1.16 and 1.216 Å for the La^{3+} ion [43].

With the relaxed geometry obtained above, the ground-state electronic band structures for $LaSi_3N_5$:Ce, $La_3Si_6N_{11}$:Ce_{2a}, and $La_3Si_6N_{11}$:Ce_{4c} have been calculated. The corresponding total energies are listed in Table IV. The values of $La_3Si_6N_{11}$:Ce_{2a} and $La_3Si_6N_{11}$:Ce_{4c} are quite similar, with $La_3Si_6N_{11}$:Ce_{2a} being favored only by 0.3 mHa (less than 10 meV), which indicates that the Ce^{3+} ions should nearly equally occupy the La_{2a} and La_{4c} sites in $La_3Si_6N_{11}$ at firing temperature(1500 °C–2000 °C). Moreover, there are twice more asymmetric sites than symmetric sites in $La_3Si_6N_{11}$. Hence there should be twice more Ce^{3+} lying in La_{4c} sites than in La_{2a}. This result is consistent with experimental observation that shows the Ce^{3+} can equally substitute on the La_{2a} and La_{4c} site at high Ce concentration [16].

TABLE IV. The calculated absorption, emission, and Stokes shift of LSN phosphors, compared with the experimental data [13,15].

Case	$LaSi_3N_5$:Ce	$La_3Si_6N_{11}$:Ce_{2a}	$La_3Si_6N_{11}$:Ce_{4c}
A_0	−763.4608 Ha	−932.1088 Ha	−932.1091 Ha
A_0^*	−763.3323 Ha	−932.0062 Ha	−932.9887 Ha
A^*	−763.3379 Ha	−932.0129 Ha	−932.0924 Ha
A	−763.4524 Ha	−932.1011 Ha	−931.9968 Ha
$\Delta E_{abs}(A_0^*\text{-}A_0)$	3.50 eV	2.79 eV	3.28 eV
ΔE_{abs}(Exp.)	3.43 eV	2.58 eV	–
$\Delta E_{em}(A^*\text{-}A)$	3.12 eV	2.40 eV	2.60 eV
ΔE_{em}(Exp.)	2.95 eV	2.25 eV	–
ΔS(Cal.)	3080 cm^{-1}	3160 cm^{-1}	5456 cm^{-1}
ΔS(Exp.)	3815 cm^{-1}	2717 cm^{-1}	–

Figure 7 (left-hand, upside) shows the Kohn-Sham DFT band structure results, in the ground state (supercell). Compared with the bulk results shown in Fig. 4, for the primitive cell, a localized Ce_{4f} state occurs in the band gap. In this case, no Ce_{5d} state appears into the band gap, as indicated in Fig. 7 (right-hand, upside). Thanks to partial density of states plotting as shown in Figs. 8(a)–8(c), the composition of CBM for the LSN phosphors has been determined to be a hybrid state of La_{4f} and La_{5d}, similar to the result of the corresponding LSN bulk. This result is not consistent with the experimental fact that both LSN phosphors give an intense emitting light, for which a localized Ce_{5d} state, inside the band gap, is expected. The reason for this failure is an incorrect identification of the levels in a ground-state electronic band structure, provided by DFT (or even quasiparticle band structure) with the experimentally observed neutral excitation of the system. Indeed, during the absorption process, the Ce_{4f} electron is promoted to the Ce_{5d} state and a hole is left. Due to the localized nature of the Ce_{4f} state, there is a strong Coulomb attraction between the promoted Ce_{5d} electron and the hole in the Ce_{4f} state. This electron-hole interaction will pull the Ce_{5d} state to a lower energy, which is not depicted in a standard ground-state DFT band structure.

B. Excited state

As shown by the ground-state calculations, the electron-hole interaction is necessary to describe the excited state of the LSN phosphor. In our work, the electron-hole interaction is described in the constrained DFT method. Figure 7 (A_0^* case) depicts the results for LSN phosphors. When one hole is created in the $4f$ band, the Ce_{5d} state successfully appears below the CBM of the LSN host. Eigenenergies from the DFT calculations cannot be identified as the optical transition levels for the neutral excitation. Instead of comparing eigenenergies, the neutral excitation energy can be calculated from the ΔSCF method through the total energy difference of the ground state and excited state. The calculated absorption energies for $LaSi_3N_5$:Ce, $La_3Si_6N_{11}$:Ce_{2a}, and $La_3Si_6N_{11}$:Ce_{4c} are shown in Table IV, and will be used to identify the luminescent center in the two LSN phosphors.

C. Lattice relaxation in the excited state

Following the configuration coordinate diagram in Fig. 2, after absorption, the system will be out of equilibrium due to the change in electronic configuration, leading to the relaxation of atomic position in the excited state. Accordingly, we have conducted geometry optimization of doped LSN phosphors. The constrained DFT has been used to keep the electronic configuration of Ce^{3+} ion in its excited state. In the geometry optimization, the lattice parameters have been fixed to the value from the ground state, because the time scale of atomic position relaxation is much shorter than the change of the macroscopic state (strain) of the crystal [21,42]. Figure 7 (A^* case) shows the band structure for the excited state of emission process, and the corresponding partial density of states are depicted in the Figs 8(d)–8(f). Also, the charge density at the Γ point of the lowest band over the Ce_{4f} state is shown in Fig. 9. For the case of $La_3Si_6N_{11}$:Ce_{4c},

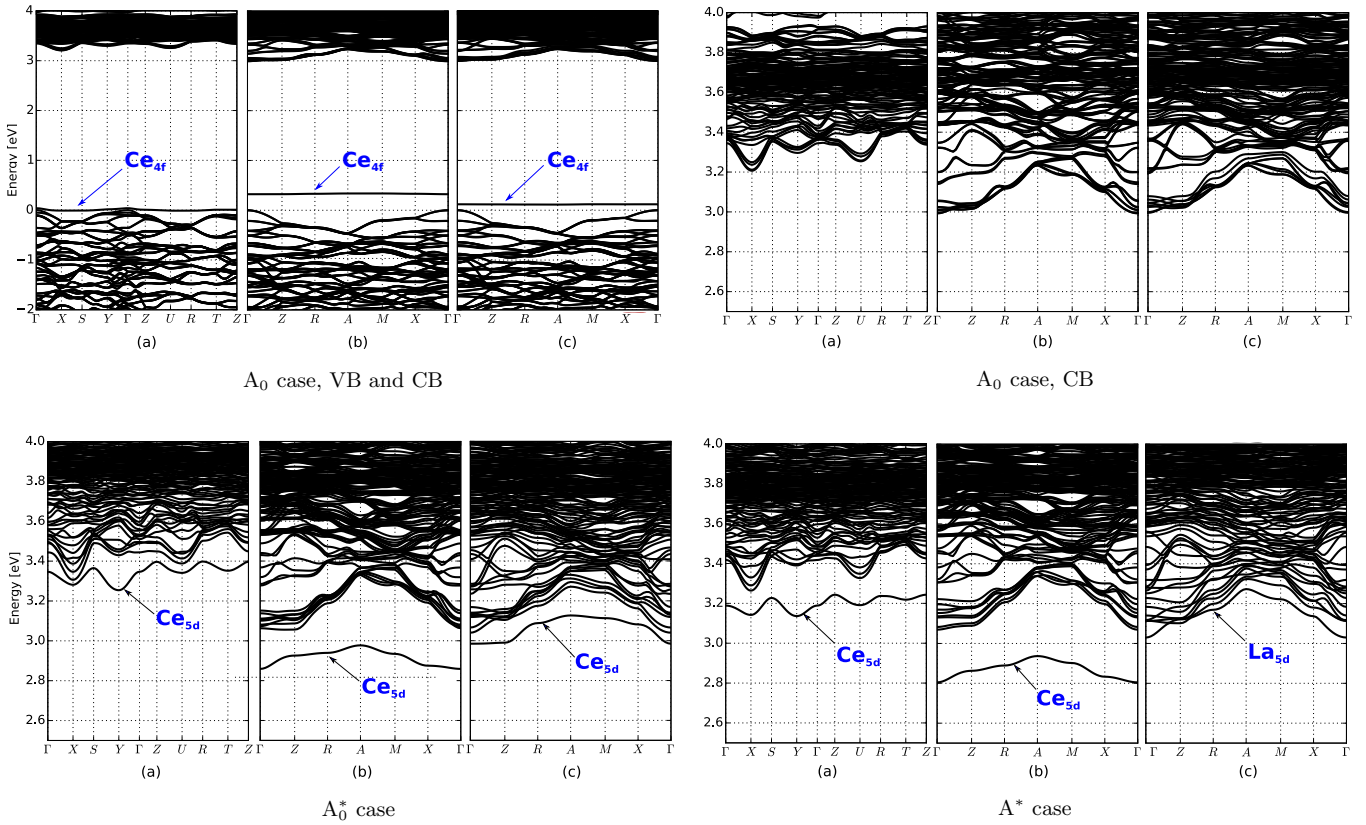

FIG. 7. Electronic band structure of ground state A_0 case, valence band (VB), and conduction band (CB); ground state A_0 case, CB; excited state A_0^* case, with ground-state geometry; excited-state A^* case, with excited-state geometry. (a) $LaSi_3N_5$:Ce; (b) $La_3Si_6N_{11}$:Ce_{2a}; and (c) $La_3Si_6N_{11}$:Ce_{4c}.

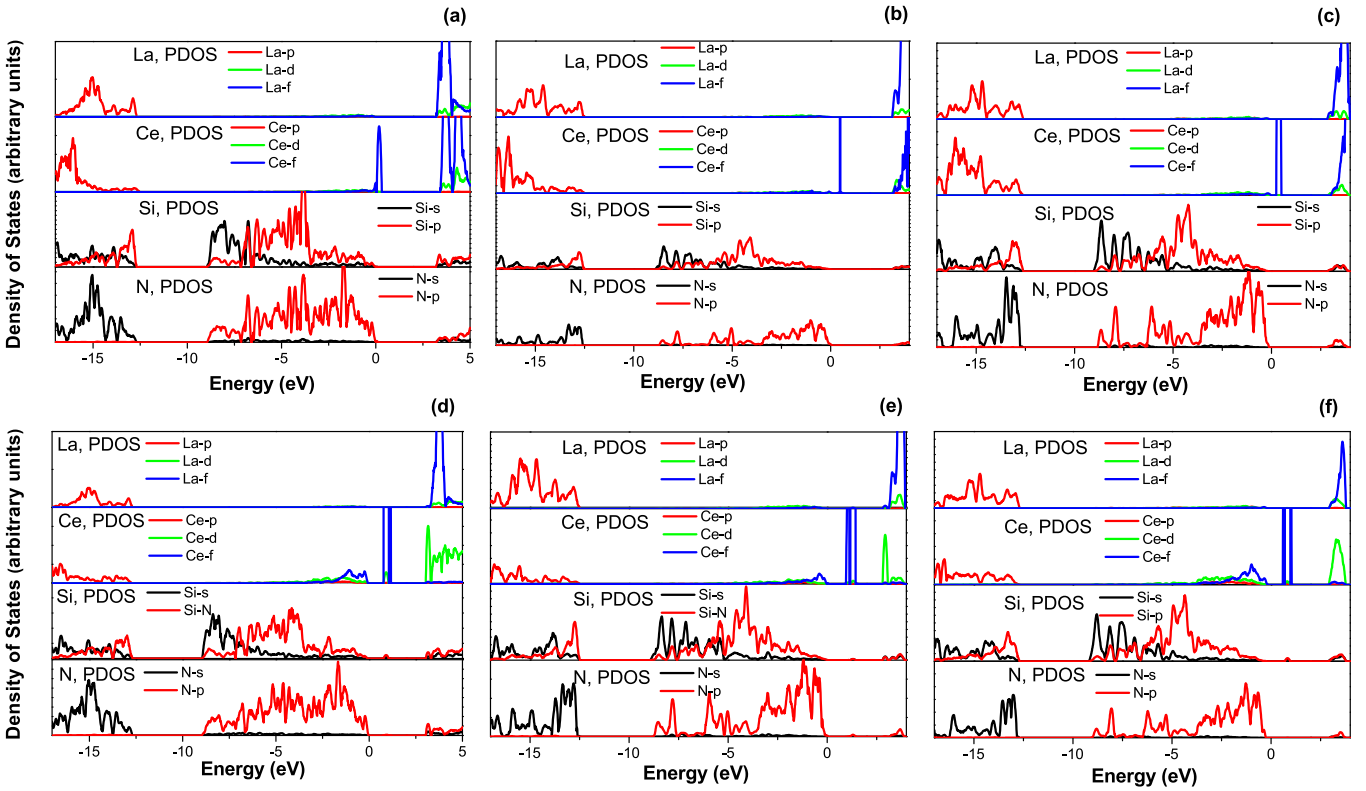

FIG. 8. Partial density of state of LSN:Ce phosphors: (a) $LaSi_3N_5$:Ce,A_0; (b) $La_3Si_6N_{11}$:Ce_{2a}, A_0; (c) $La_3Si_6N_{11}$:Ce_{4c}, A_0; (d) $LaSi_3N_5$:Ce,A^*; (e) $La_3Si_6N_{11}$:Ce_{2a}, A^*; and (f) $La_3Si_6N_{11}$:Ce_{4c}, A^*.

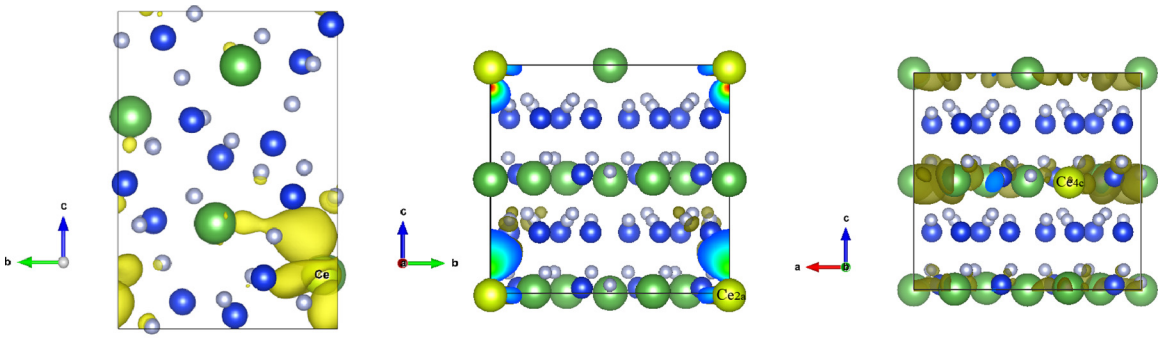

(a) $LaSi_3N_5$:Ce (b) $La_3Si_6N_{11}$:Ce_{2a} (c) $La_3Si_6N_{11}$:Ce_{4c}

FIG. 9. Charge density at Γ point of (a) the 200th band of $LaSi_3N_5$:Ce (yellow isosurface); (b) the 232nd band of $La_3Si_6N_{11}$:Ce_{2a} (blue and red isosurface, and some small yellow isosurface); and (c) the 232nd band of $La_3Si_6N_{11}$:Ce_{4c} (yellow isosurface).

the lowest conduction band has La_{5d} character, while those of $LaSi_3N_5$:Ce and $La_3Si_6N_{11}$:Ce_{2a} are composed of Ce_{5d} state. Based on the above calculation, we have obtained the theoretical emission energies and Stokes shifts for the $LaSi_3N_5$:Ce and $La_3Si_6N_{11}$:Ce, that are listed in Table IV. Through the comparison with the experimental value for the LSN phosphor, we can deduce that the luminescence center for the $LaSi_3N_5$:Ce and $La_3Si_6N_{11}$:Ce phosphors is from the Ce_{La} and Ce_{2a} site, respectively. For the case of $La_3Si_6N_{11}$:Ce_{4c}, we tentatively assign this Ce site as nonluminescent center with the Ce_{5d} states inside the conduction bands, as we discussed in our work for other phosphors [21]. Although more advanced methods like the GW approximation might be needed to precisely determine the relative position of Ce_{5d} and the CBM, this is out of the scope of this work [44]. Here, it is worthy to note that the calculated Stokes shift for $LaSi_3N_5$:Ce is underestimated compared to the experimental data, while the calculated value for $La_3Si_6N_{11}$:Ce is overestimated. The reason for the above difference is due to the relative accuracy of the theoretical method, which gives an error about 0.2 eV for the transition energies, while the accurate value of Stokes shift is smaller than 0.5 eV.

We observe that, with such an excited structure geometry, the Stokes shift and emission energy are in reasonable agreement with experimental data. At this stage, the effect of the excited state relaxation of atomic positions can be analyzed. One can focus on the change of Ce^{3+} coordination environment in the $LaSi_3N_5$ and $La_3Si_6N_{11}$, as listed in Table V. The change of Ce-N bond length is due to the movement of ions in the crystal structure. For $LaSi_3N_5$, an anisotropic distortion occurs around the Ce^{3+} ion. Four bond lengths are increased (by up to 6% for Ce-$N1^b$), while five bond lengths are decreased (by up to 5% for Ce-$N2^b$ and Ce-$N5^b$). For $La_3Si_6N_{11}$:Ce_{2a} there is a slight shortening of the Ce-N1 bond length, and a larger shortening of the Ce-N2 bond length (3%). Finally, for $La_3Si_6N_{11}$:Ce_{4c}, all bond lengths contract, by up to nearly 7% for Ce-N4. These information can be useful for the analysis of emission color of Ce^{3+} ion in the two LSN compounds.

Now, we can come back to the analysis of the behavior of the eigenenergy difference between the Ce_{5d} band and the bottom of the conduction band. We will show that it can increase as well as decrease upon relaxation, depending on the behavior of the energy difference between the Ce_{4f} band and the bottom of the conduction band, and the bonding or antibonding character of the Ce_{5d} orbital. For this purpose, we first define the total energy $E(\mathbf{R}, f_{5d})$ as a function of the Ce_{5d} occupation number, denoted f_{5d}, and at atomic positions symbolically denoted as

TABLE V. Ce-N bond lengths (Å) of the Ce site. The bold characters highlight the biggest change of local geometry of three Ce^{3+} sites, as mentioned in the text.

$LaSi_3N_5$:Ce			
Bond	Ground	Excited	Geometry
Ce-N 1^a	3.151	3.178	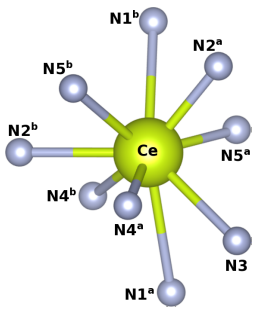
Ce-N 1^b	3.137	**3.324**	
Ce-N 2^a	2.430	2.380	
Ce-N 2^b	2.717	**2.601**	
Ce-N3	2.874	2.955	
Ce-N 4^a	2.553	2.416	
Ce-N 4^b	2.898	2.835	
Ce-N 5^a	2.690	2.792	
Ce-N 5^b	2.850	**2.712**	
$La_3Si_6N_{11}$:Ce_{2a}			
Ce-N1 (x4)	2.657	2.645	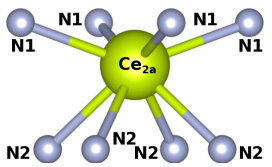
Ce-N2 (x4)	2.638	**2.555**	
$La_3Si_6N_{11}$:Ce_{4c}			
Ce-N1(x2)	2.512	2.389	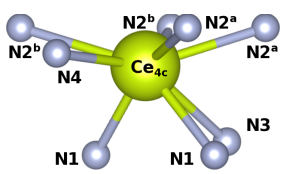
Ce-$N2^a$ (x2)	2.670	2.596	
Ce-$N2^b$ (x2)	2.901	2.895	
Ce-N3	2.802	2.718	
Ce-N4	2.641	**2.472**	

TABLE VI. Dorenbos model analysis of the [Xe]5*d* state of Ce^{3+} ion in LSN phosphors. GS: ground state; EX: excited state.

–	$LaSi_3N_5$:Ce	$La_3Si_6N_{11}$:Ce_{2a}	$La_3Si_6N_{11}$:Ce_{4c}
χ_{av}	1.74	1.68	1.68
α_{sp}^N	7.07	7.52	7.52
ε_c, GS	21380 cm^{-1}	25166 cm^{-1}	23671 cm^{-1}
ε_c, EX	23950 cm^{-1}	28242 cm^{-1}	–
β	5.67×10^8	1.20×10^9	1.20×10^9
R_{av}, GS	281 pm	265 pm	270 pm
R_{av}, EX	280 pm	260 pm	–
ε_{cfs}, GS	7181 cm^{-1}	17088 cm^{-1}	16461 cm^{-1}
ε_{cfs}, EX	7232 cm^{-1}	17751 cm^{-1}	–

R. Note that the occupation of the Ce_{4f} levels decrease at the same rate as the occupation of the Ce_{5d} increases. Due to Janak's theorem [45], the derivative of the total energy with respect to the Ce_{5d} occupation number is directly linked to the difference between Ce_{5d} and Ce_{4f} eigenvalues, as well as to their differences with respect to the conduction band minimum, $\frac{\partial E(\mathbf{R}, f_{5d})}{\partial f_{5d}} = \epsilon_{5d} - \epsilon_{4f} = (\epsilon_{5d} - \epsilon_{\mathrm{CBM}}) - (\epsilon_{4f} - \epsilon_{\mathrm{CBM}})$. In the exact density functional theory, the eigenenergies themselves should not depend on the occupation numbers, while in semilocal approximations, a convexity is observed [46]. Actually, this convexity is quite important, and we have argued in the previous subsection that the difference of total energies is more reliable than eigenenergies to predict excited states and their relaxation. Still, if the eigenenergies were constant, $E(\mathbf{R}, f_{5d} = 1) - E(\mathbf{R}, f_{5d} = 0) = (\epsilon_{5d} - \epsilon_{\mathrm{CBM}}) - (\epsilon_{4f} - \epsilon_{\mathrm{CBM}})$. Comparing the relaxed and unrelaxed geometries, we see that the Stokes shift is approximately equal to the change of $\epsilon_{5d} - \epsilon_{\mathrm{CBM}}$ minus the change $\epsilon_{4f} - \epsilon_{\mathrm{CBM}}$ upon relaxation. Thus, if the Ce_{4f} eigenenergy increases significantly with respect to the conduction band, due to the relaxation, and in particular, if this increase is bigger than the Stokes shift, it might be that the Ce_{5d} raises with respect to the conduction band. We have checked that this is indeed the case for $La_3Si_6N_{11}$:Ce_{4c}. Physically, we know that the electronic negative charge that is present on the Ce_{4f} in the ground state repels the negatively charge N ions. When the Ce_{4f} gets unoccupied, a large contraction of the N cage is observed, as described in the previous subsection. If the Ce_{5d} is more antibonding than the La_{5d} states at the bottom of the conduction band, the eigenenergy difference between them will decrease.

D. Analysis based on the Dorenbos model with first-principles geometry data

The Dorenbos model described in Appendix has been used to analyze the different luminescent behavior of $LaSi_3N_5$:Ce and $La_3Si_6N_{11}$:Ce. The structural geometries of the ground and excited states, as depicted in Table V, were adopted to obtain the R_i and R_{av} in the corresponding formula. The results about the centroid shift of the 5*d* energy, ε_c, are listed in Table VI. At present, the ε_c analysis of $La_3Si_6N_{11}$:Ce_{4c} in the emission state was not conducted, since this site was determined to be nonluminescent. For the cases of $LaSi_3N_5$:Ce and $La_3Si_6N_{11}$:Ce_{2a}, the obtained results indicate that the difference in ε_c is 0.47 and 0.5 eV, for the ground and excited states, respectively.

Qualitative analysis also has been performed on the crystal-field splitting, ε_{cfs}. In our cases, the coordination environment of Ce^{3+} ion in $LaSi_3N_5$:Ce is in the form of tricapped trigonal prism, while those of Ce_{2a} and Ce_{4c} in $La_3Si_6N_{11}$:Ce can be seen as distorted cubic (square antiprism and bicapped trigonal prism, respectively). Following this idea, the ε_{cfs} in the two nitrides can be calculated through the β, fitted according to Ref. [8]. The corresponding results are also listed in Table VI. Similar with the situation of ε_c, the analysis of $La_3Si_6N_{11}$:Ce_{4c} in the emission state was not conducted. If we assume r(LSN) to be equal to 2.4, the effect of ε_{cfs} on the cases of $LaSi_3N_5$:Ce and $La_3Si_6N_{11}$:Ce_{2a}, give an energy difference of 0.51 and 0.53 eV, for the ground and excited states, respectively.

Through the analyses above, the difference of redshift between the $LaSi_3N_5$:Ce and $La_3Si_6N_{11}$:Ce_{2a}, is calculated to be 0.98 and 1.03 eV for the ground and excited states that compares reasonably with the experimental data of 0.81 and 0.72 eV, respectively. The calculated Stokes shift is 2600 and 3466 cm^{-1} for the $LaSi_3N_5$:Ce and $La_3Si_6N_{11}$:Ce_{2a}. Considering the qualitative character of Dorenbos model, these values are quite reasonable. Based on the above consistence, we can give the conclusion in two aspects: firstly, the structural geometry for LSN phosphor are accurately described, not only for the ground state, but also for the excited state. Second, the difference of luminescence in $LaSi_3N_5$:Ce and $La_3Si_6N_{11}$:Ce_{2a} could be ascribed to the larger spectroscopic polarization of N^{3-} ion in $La_3Si_6N_{11}$ [17,18], and the stronger crystal-field splitting of Ce_{2a} site.

V. CONCLUSION

In this paper, an *ab initio* study has been conducted to accurately describe the neutral excitation of Ce^{3+} ions in two nitrides, $LaSi_3N_5$ and $La_3Si_6N_{11}$. The analysis of Ce^{3+} luminescence follows from the configurational coordinate diagram, in which the ground-state and excited-state descriptions rely on the DFT+U and the constrained DFT approach. The absorption and emission energies are calculated with the ΔSCF method. Following these methods, the Stokes shift can be obtained. The luminescent centers (Ce_{La} and Ce_{2a}) can be identified from the agreement between the theoretical calculation and experimental results. It remains to be seen whether the same method can be applied successfully to other phosphors. For this purpose, other materials for which experimental data are known should be analyzed. This should be followed by large-scale computations for new dopant-hosts combinations.

ACKNOWLEDGMENTS

We acknowledge discussions with D. Waroquiers, and thank J.-M. Beuken for computational help. This work, done in the framework of ETSF (project No. 551), has been supported by the Fonds de la Recherche Scientifique (FRS-FNRS Belgium) through a FRIA fellowship (S.P.) and the PdR Grant No. T.0238.13 - AIXPHO. Computational resources have been provided by the supercomputing facilities of the Université catholique de Louvain (CISM/UCL) and the

Consortium des Equipements de Calcul Intensif en Fédération Wallonie Bruxelles (CECI) funded by the FRS-FNRS under Grant No. 2.5020.11.

APPENDIX: THE DORENBOS MODEL

To explain the different optical performance between $LaSi_3N_5$:Ce and $La_3Si_6N_{11}$:Ce_{2a}, a qualitative analysis has been performed based on the semiempirical model proposed by Dorenbos [7–9] and the corresponding structural geometry obtained from this work, including the consideration of ground state as well as the excited state.

First, it is worthy to briefly introduce the Dorenbos model here. Figure 10 shows the basic idea. The redshift of the first $4f \rightarrow 5d$ transition D(A) in the compound A, can be written as

$$D(A) = \varepsilon_c(A) + \frac{1}{r(A)}\varepsilon_{cfs}(A) - 1890\ \mathrm{cm}^{-1} \quad \text{(A1)}$$

in which the ε_c(A) is the centroid shift of the $5d$ energy relative to the free ion, defined as follows:

$$\varepsilon_c(A) = 1.44 \times 10^{17} \Sigma_{i=1}^{N} \frac{\alpha_{sp}^{i}}{R_i^6}. \quad \text{(A2)}$$

In the above formula, α_{sp}^{i} is the spectroscopic polarization of anion i located at distance of R_i from the Ce^{3+} ion in the relaxed structure. The summation is over all anions N in the coordinated environment. For nitrides, the qualitative relationship between α_{sp}^{i} and electronegativity of the cations is demonstrated as [47,48]

$$\alpha_{sp}^{N} = 0.87 + \frac{18.76}{\chi_{av}^2}, \quad \text{(A3)}$$

where the electronegativity is

$$\chi_{av} = \frac{1}{N}\Sigma_{i=1}^{M}\frac{Z_i\chi_i}{\gamma}. \quad \text{(A4)}$$

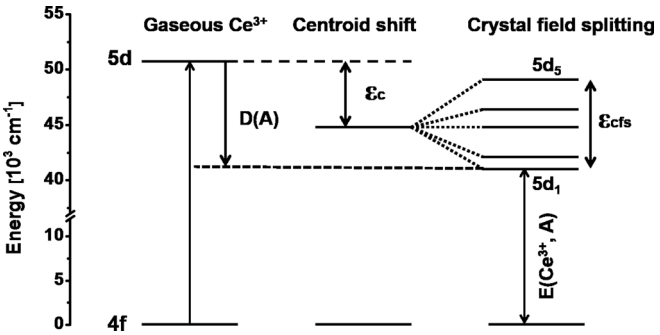

FIG. 10. Dorenbos model on the energy of [Xe]$5d$ electron configuration of Ce^{3+} ion. The ε_c(A), ε_{cfs}(A), and D(A) indicate the centroid shift, crystal-field splitting, and redshift of Ce_{5d} energy level in compound A, respectively [8].

This formula is obtained from the reason that a cation of formal charge $+Z_i$ will bind on average with Z_i/γ anions of formal charge of $-\gamma$. The summation is over all cations M in the compound, and N is the number of anions [9,47].

Another parameter affecting the spectroscopic redshift is the contribution from the crystal-field shift, $\frac{1}{r(A)}\varepsilon_{cfs}$(A). The crystal-field splitting ε_{cfs}(A) is defined as the energy difference between the lowest and highest $5d$ level. A fraction $1/r$(A) contributes to the redshift, where r(A) usually varies between 1.7 and 2.4. The ε_{cfs}(A) is determined as

$$\varepsilon_{cfs} = \frac{\beta}{R_{av}^2} \quad \text{(A5)}$$

in which β is a parameter related to the shape and size of the anion polyhedron coordinated to the Ce^{3+} ion, and R_{av} is average distance between the Ce^{3+} ion and anions in the relaxed structure. In our work, the Dorenbos model has been used to analyze the different luminescent behavior of $LaSi_3N_5$:Ce and $La_3Si_6N_{11}$:Ce.

[1] H. Hoppe, Angew. Chem. Int. Edit. **48**, 3572 (2009).
[2] M. Zeuner, S. Pagano, and W. Schnick, Angew. Chem. Int. Edit. **50**, 7754 (2011).
[3] Y. Jia, H. Qiao, Y. Zheng, N. Guo, and H. You, Phys. Chem. Chem. Phys. **14**, 3537 (2012).
[4] M. Krings, G. Montana, R. Dronskowski, and C. Wickleder, Chem. Mater. **23**, 1694 (2011).
[5] A. Setlur, E. Radkov, C. Henderson, J. Her, A. Srivastava, N. Karkada, M. Kishore, N. Kumar, D. Aesram, A. Deshpande, B. Kolodin, L. Grigorov, and U. Happek, Chem. Mater. **22**, 4076 (2010).
[6] T. Suehiro, N. Hirosaki, and R. Xie, ACS Appl. Mater. Inter. **3**, 811 (2011).
[7] P. Dorenbos, Phys. Rev. B **62**, 15640 (2000).
[8] P. Dorenbos, Phys. Rev. B **62**, 15650 (2000).
[9] P. Dorenbos, Phys. Rev. B **65**, 235110 (2002).
[10] Z. Inoue, M. Mitomo, and N. Li, J. Mater. Sci. **15**, 2915 (1980).
[11] M. Woike and W. Jeitschko, Inorg. Chem. **34**, 5105 (1995).
[12] H. Yamane, T. Nagura, and T. Miyazaki, Acta Cryst. E **70**, i23 (2014).
[13] T. Suehiro, N. Hirosaki, R. Xie, and T. Sato, Appl. Phys. Lett. **95**, 051903 (2009).
[14] L. Cai, X. Wei, H. Li, and Q. Liu, J. Lumin. **129**, 165 (2009).
[15] N. Kijima, T. Seto, and N. Hirosaki, ECS Trans. **25**, 247 (2009).
[16] N. C. George, A. Birkel, J. Brgoch, B. C. Hong, A. A. Mikhailovsky, K. Page, A. Llobet, and R. Seshadri, Inorg. Chem. **52**, 13730 (2013).
[17] M. Mikami and N. N. Kijima, Opt. Mater. **33**, 145 (2010).
[18] M. Mikami, ECS J. Solid State Sci. Technol. **2**, R3048 (2013).
[19] S. Poncé, B. Bertrand, P. Smet, D. Poelman, M. Mikami, and X. Gonze, Opt. Mater. **35**, 1477 (2013).
[20] B. Bertrand, S. Poncé, D. Waroquiers, M. Stankovski, M. Giantomassi, M. Mikami, and X. Gonze, Phys. Rev. B **88**, 075136 (2013).
[21] S. Poncé, Y. Jia, M. Giantomassi, M. Mikami, and X. Gonze, J. Phys. Chem. C **120**, 4040 (2016).

[22] M. Marsman, J. Andriessen, and C. W. E. van Eijk, Phys. Rev. B **61**, 16477 (2000).
[23] P. Erhart, B. Sadigh, A. Schleife, and D. Åberg, Phys. Rev. B **91**, 165206 (2015).
[24] P. Erhart, A. Schleife, B. Sadigh, and D. Åberg, Phys. Rev. B **89**, 075132 (2014).
[25] I. A.M. Ibrahim, Z. Lenčéš, P. Šajgalík, and L. Benco, J. Lumin. **164**, 131 (2015).
[26] P. E. Blöchl, Phys. Rev. B **50**, 17953 (1994).
[27] X. Gonze, J. M. Beuken, R. Caracas, F. Detraux, M. Fuchs, G. M. Rignanese, L. Sindic, M. Verstraete, G. Zerah, F. Jollet, M. Torrent, A. Roy, M. Mikami, P. Ghosez, J. Y. Raty, and D. C. Allan, Comput. Mater. Sci. **25**, 478 (2002).
[28] X. Gonze, B. Amadon, P.-M. Anglade, J.-M. Beuken, F. Bottin, P. Boulanger, F. Bruneval, D. Caliste, R. Caracas, M. Côté, T. Deutsch, L. Genovese, P. Ghosez, M. Giantomassi, S. Goedecker, D. Hamann, P. Hermet, F. Jollet, G. Jomard, S. Leroux, M. Mancini, S. Mazevet, M. Oliveira, G. Onida, Y. Pouillon, T. Rangel, G.-M. Rignanese, D. Sangalli, R. Shaltaf, M. Torrent, M. Verstraete, G. Zerah, and J. Zwanziger, Comput. Phys. Commun. **180**, 2582 (2009).
[29] M. Torrent, F. Jollet, F. Bottin, G. Zérah, and X. Gonze, Comput. Mater. Sci. **42**, 337 (2008).
[30] J. P. Perdew, K. Burke, and M. Ernzerhof, Phys. Rev. Lett. **77**, 3865 (1996).
[31] A. I. Liechtenstein, V. I. Anisimov, and J. Zaanen, Phys. Rev. B **52**, R5467 (1995).
[32] F. Jollet, M. Torrent, and N. Holzwarth, Comput. Phys. Commun. **185**, 1246 (2014).
[33] J. Gracia, L. Seijo, Z. Barandiaran, D. Curulla, H. Niemansverdriet, and W. van Gennip, J. Lumin. **128**, 1248 (2008).
[34] J. L. Pascual, J. Schamps, Z. Barandiaran, and L. Seijo, Phys. Rev. B **74**, 104105 (2006).
[35] G. Onida, L. Reining, and A. Rubio, Rev. Mod. Phys. **74**, 601 (2002).
[36] A. Canning, A. Chaudhry, R. Boutchko, and N. Grønbech-Jensen, Phys. Rev. B **83**, 125115 (2011).
[37] A. Chaudhry, R. Boutchko, S. Chourou, G. Zhang, N. Grønbech-Jensen, and A. Canning, Phys. Rev. B **89**, 155105 (2014).
[38] A. Chaudhry, A. Canning, R. Boutchko, M. J. Weber, N. Grønbech-Jensen, and S. E. Derenzo, J. Appl. Phys. **109**, 083708 (2011).
[39] D. J. Tozera and N. C. HandyI, Phys. Chem. Chem. Phys. **2**, 2117 (2000).
[40] R. Martin, *Electronic Structure: Basic Theory and Practical Methods* (Cambridge University Press, Cambridge, 2004).
[41] A. Alkauskas, B. B. Buckley, D. D. Awschalom, and C. G. V. de Walle, New J. Phys. **16**, 073026 (2014).
[42] R. Blasse and C. Grabmaier, *Luminescent Materials* (Springer, Berlin, Heidelberg, 1994).
[43] R. D. Shannon and C. T. Prewitt, Acta Crystallogr. Sect. B **25**, 925 (1969).
[44] F. Aryasetiawan and O. Gunnarsson, Rep. Prog. Phys. **61**, 237 (1998).
[45] J. F. Janak, Phys. Rev. B **18**, 7165 (1978).
[46] M. Cococcioni and S. de Gironcoli, Phys. Rev. B **71**, 035105 (2005).
[47] T. Wang, Z. Xia, Q. Xiang, S. Qin, and Q. Liu, J. Lumin. **166**, 106 (2015).
[48] T. Wang, Q. Xiang, Z. Xia, J. Chen, and Q. Liu, Inorg. Chem. **55**, 2929 (2016).